Acta Geologica Polonica, Vol. 59 (2009), No. 1, pp. 93–109

The comparison of alteration zones in the Sungun porphyry copper deposit, Iran (based on fluid inclusion studies)

OMID ASGHARI[1], ARDESHIR HEZARKHANI[2] AND FATEMEH SOLTANI[3]

[1]*Department of mining engineering, University of Kashan, Kashan, Iran. E-mail: O.asghari@aut.ac.ir*
[2]*Department of Mining and Metallurgy Engineering, Amirkabir University of Technology, Tehran, P.O.Box 45875-4413,424 Hafez Ave., Tehran, Iran. E-mail: ardehez@aut.ac.ir*
[3]*Department of Mining and Metallurgy Engineering, Amirkabir University of Technology, Tehran, Iran. E-mail: Zohrehs61@yahoo.com.*

ABSTRACT:

Ashgari, O., Hezarkhani, A. and Soltani, F. 2009. The comparison of alteration zones in the Sungun porphyry copper deposit, Iran (based on fluid inclusion studies). *Acta Geologica Polonica*, **59** (1), 93–109. Warszawa.

The Sungun porphyry copper deposit (PCD) is located in East Azarbaijan, in northwestern Iran. The felsic rocks occur as stocks and dykes ranging in composition from quartz monzodiorite through quartz monzonite. The stocks are classified into porphyry stocks I and II. Porphyry stock II, hosting the copper ore, experienced an intense hydro-fracturing leading to the formation of stockwork-type veinlets and micro-veinlets of quartz, sulphides, carbonates and sulphates. Three distinct types of hydrothermal alteration and sulphide mineralization are recognized at Sungun (1) hypogene, (2) contact metasomatic (skarn), and (3) supergene. Hypogene alteration is developed in four kinds: potassic, phyllic, propylitic and argillic. Three types of fluid inclusions are typically observed at Sungun: (1) vapour-rich, two-phase, (2) liquid-rich two-phase and (3) multi-phase. Halite is the principal solid phase in multiphase inclusions. Primary multiphase inclusions (LVH type fluid inclusions) within the quartz crystals in quartz-sulphide and quartz-molybdenite veinlets (quartz associated with sulphide minerals) were selected for micro-thermometric analyses and considered to be suitable for pressure calculations and estimation of hydrothermal fluid density. Homogenization temperature, salinity, pressure and density were measured and calculated in forty-seven selected samples

None of the variables could distinguish the potassic from phyllic alteration zones clearly. In the potassic alteration zone, the average of homogenization temperature is about 413°C, while in the phyllic alteration zone its average is about 375 °C. It was expected that the temperature in the potassic alteration zone would be higher than that in the phyllic zone, but the difference found was not very significant The fluid inclusion salinity within both alteration zones obviously relates to their homogenization temperature: the average salinity in the samples from the potassic zone is 46.3 (wt% NaCl equiv.), which is higher than that in the samples from the phyllic zone.. Based on the estimated depth of the potassic alteration domain, it is expected that the lithostatic pressure was higher than in the phyllic alteration zone. According to the fluid inclusion studies and pressure calculation, it is estimated that the average pressure for the potassic alteration zone was about 512 (bars) while the average pressure for phyllic zone was about 310 (bars). The average density of fluids in the samples from the potassic alteration zone is 1.124 (g/cm^3), which is higher than that in the phyllic alteration zone (1.083 g/cm^3).

Key words: Fluid inclusion; Porphyry copper deposit; Potassic alteration; Phyllic alteration.

INTRODUCTION

Porphyry copper deposits are generated where magmatic–hydrothermal fluids are expelled from a crystallizing felsic magma (Burnham 1979; Ulrich *et al.* 2001). Cooling, depressurization, and reaction between the fluids and the wall rocks cause metals to precipitate in and around the fractures, forming veins with alter-

ation envelopes. Alteration assemblages and associated mineralization in porphyry ore deposits develop from massive hydrothermal systems dominated by magmatic and meteoric fluids (Sillitoe 1997; Hedenquist and Richards 1998). These systems develop in and adjacent to subvolcanic porphyritic intrusions that are apophyses to deeper-seated magma bodies (Dilles and Einaudi 1992; Sillitoe and Hedenquist 2003; Heinrich *et al.* 2003). Based on the fluid inclusion analyses, it seems that the parental fluids could be trapped within the porphyry Cu deposits and the inclusions show both halite-saturated brines (LVH types) and low-salinity vapour inclusions (Nash 1976; Roedder 1984; Bodnar 1995; Tosdal and Richards 2001; Heinrich 2005).The formation of brine and vapour is inferred to result from a miscibility gap in the $NaCl–H_2O$ system that coincides with the pressure (< 2200 bars) and temperature (300 to 600 °C) at which most porphyry Cu deposits form (Sourirajan and Kennedy 1962; Urusova 1975; Roedder and Bodnar 1980; Bodnar *et al.* 1985; Beane and Bodnar 1995; Kehayov *et al.* 2003).

Fluid inclusion studies in porphyry copper deposits (PCDs) have proven to be an important tool to constrain the physico-chemical conditions of the hydrothermal fluids responsible for vast and pervasive alteration and mineralization processes. These fluid inclusion studies have shown many common features in such deposits throughout the world (Nash 1976; Chivas and Wilkins 1977; Beane and Titley 1981; Roedder 1984; Quan *et al.* 1987; Beane and Bodnar 1995; Ulrich *et al*. 2001; Redmond *et al*. 2004).

In the Sungun PCD, numerous cross-cutting quartz veinlets and micro-veinlets, developed in various stages of alteration and mineralization, provided suitable material for fluid inclusions studies. Etminan (1977) was the first to recognize the presence of porphyry-type copper mineralization at Sungun on the basis of fluid inclusion studies. Based upon a systematic sub-surface sampling, more detailed studies of fluid inclusions were carried out by Mehrpartou (1993) and Calagari (1997) and comprehensive microthermometric data were compiled Additional fluid inclusion work on the Sungun PCD was done by Hezarkhani and Williams-Jones (1998), Hezarkhani *et al.* (1999) and Hezarkhani (2006a).

In the present research, we illustrate the differences between two potassic and phyllic alterations based on fluid inclusion data. As expected, all variables such as homogenization temperature, salinity, pressure and density have higher average values in the potassic than in the phyllic alteration zones. However, it will be shown that none of these parameters derived from the microthermometry of fluid inclusions can individually enable the discrimination of potassic from phyllic alteration.

GEOLOGICAL SETTING

Although porphyry copper deposits have been intensively studied in the Mesozoic–Cenozoic orogenic belts of the American Cordillera and East Pacific Rim and their genesis is relatively well understood, there have been few studies of this style of mineralization in Iran and other countries of Asia. In Iran, al1 known porphyry copper mineralization occurs in the Cenozoic Sahand-Bazman orogenic belt (Text-fig. 1). This belt was formed by subduction of the Arabian plate beneath central Iran during the Alpine orogeny (Berberian 1981). Subduction and subsequent continental collision during the Paleocene to Oligocene caused extensive alkaline and calc-alkaline volcanic and plutonic igneous activity (Shahabpour 1982; Berberian l983), including intrusion of a porphyritic calc-alkaline stock at Sungun during Miocene time (Mehrparto 1993).

The Sungun PCD is located about 100 km northeast of Tabriz, in the northwestern part of Iran. The Sungun porphyries intruded Upper Cretaceous carbonate rocks, a series of Eocene arenaceous-argillaceous rocks, and a series of Oligocene dacitic breccias, tuffs and trachy-andesitic lavas (Emami and Babakhani 1991; Mehrpartou 1993, Hezarkhani 1998, 2006a, 2006b). The Sungun porphyries, which contain >500 Mt of sulphide ore grading 0.76 percent Cu and ~0.01 percent Mo, occur as stocks and dykes, and are a series of calc-alkaline igneous rocks with a typical porphyritic texture (Hezarkhani and Williams-Jones 1998). They are situated in the northwestern part of a NW–SE trending Cenozoic magmatic belt (Sahand-Bazman) within which the Sarcheshmeh PCD is also located. The Sar Cheshmeh porphyry copper mine is in the Central Iranian Volcanic Belt (CIVB), in the Kerman Province of Iran. The deposit contains 1200 million tons ore of 0.69% Cu and 0.03% Mo (Shahabpour and Doorandish 2007) (see inset in Text-fig. 1). The Sungun stocks are divided into two groups: porphyry stock I is quartz monzodiorite; porphyry stock II (the subject of this study) hosts the Sungun PCD and varies in composition from quartz monzonite through granodiorite to granite. Four series of cross-cutting dykes varying in composition from quartz monzodiorite to granodiorite intersect the Sungun stocks.

HYDROTHERMAL ALTERATION AND MINERALIZATION

Alteration assemblages and related mineralization in the Sungun porphyry copper deposit have been investigated by geological mapping, and de-

tailed studies of the mineralogy, petrography and chemistry of a large number of borehole cores and outcrop samples from various parts of the stock (Text-fig. 2). Hydrothermal alteration and mineralization at Sungun are centred on the stock and were broadly synchronous with its emplacement. Early hydrothermal alteration was dominantly potassic and propylitic, and it was followed by later phyllic and argillic alteration (Hezarkhani and Williams-Jones 1998).

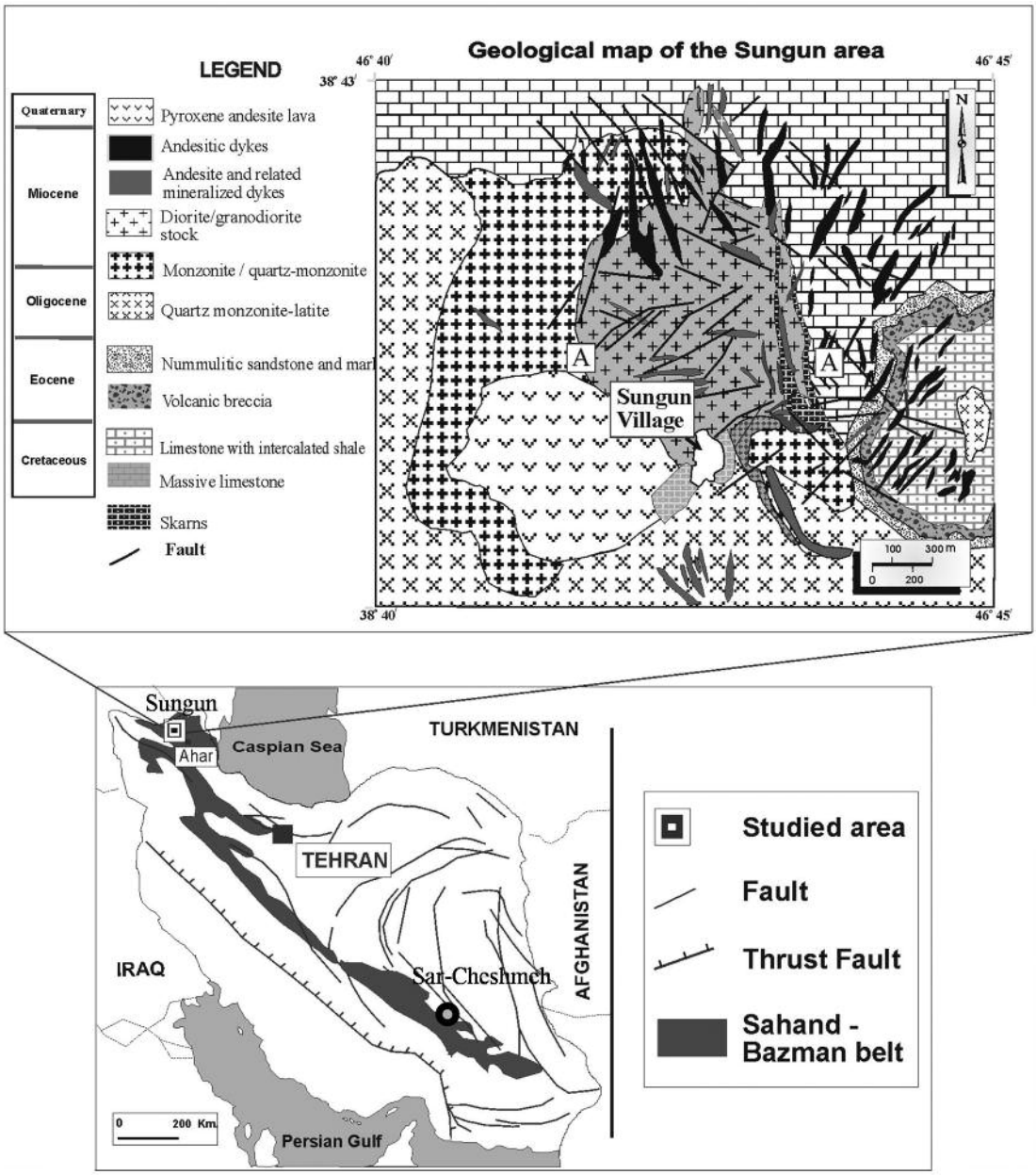

Text-fig. 1. Geological map of Iran (modified from: Stocklin 1977; Shahabpour and Doorandish, 2007) showing the Sahand-Bazman belt: Calc-alkaline volcanic and quartz monzonite and quartz diorite intrusions of predominantly Miocene age, hosting Cu-Mo porphyry mineralization and geological map of the Sungun deposit area, showing field relationships among the various subtypes of Sungun intrusive rocks, and the outline of the mineralized zone. The porphyritic quartz monzonite rims all other porphyritic plutons to the south and west, and Cretaceous limestone and associated skarn border the north and east. Andesite and andesitic dykes are distributed through the northern and western parts of the deposit (mainly outside the stock). Mineralized dykes intrude the quartz monzonite stock in the central part of the deposit. Skarn-type alteration (and associated mineralization) occurs predominantly adjacent to the eastern margin of the stock (modified from Mehrpartou 1993 and Hezarkhani 2006a)

Potassic alteration

The earliest alteration is represented by potassic mineral assemblages developed pervasively and as halos around the veins in the deep and central parts of the Sungun stock (Hezarkhani and Williams-Jones 1998). The potassic alteration is characterized by the occurrence of K feldspar and displays a close spatial association with copper and molybdenum mineralization; perhaps as much as 60 percent of the copper and all of the molybdenum was emplaced during this alteration episode (Hezarkhani and Williams-Jones 1998). On average, potassically altered rocks contain 28 percent plagioclase, 33 percent orthoclase, 20 percent quartz, 15 percent ferromagnesian minerals (mainly biotite, and sericite and chlorite after biotite), and 4 percent chalcopyrite, pyrite, zircon, scheelite, uraninite, bismuthinite, and rutile (Hezarkhani 2006a) (Text-fig. 3). Petrographic observation and electron microprobe data indicate the presence of two compositionally distinguishable types of biotite within this alteration zone: primary biotite, which is Fe enriched, brown in colour, and generally euhedral; and hydrothermal biotite, which is mainly pale brown to greenish-brown in colour, very ragged, and Mg-enriched (Table 1). The hydrothermal biotite is generally interstitial to feldspar and quartz, and locally replaced hornblende and primary biotite phenocrysts. Electron microprobe data indicate that some grains of potassium feldspar are rimmed by albite, suggesting a later transition alteration event. Quantitative study of whole-rock chemical data indicates that the principal mass changes accompanying potassic alteration were an appreciable addition of K, a small addition of Si, and a large depletion of calcium and magnesium. These reflect the replacement of plagioclase and amphibole by K feldspar and biotite respectively (Text-fig. 6a). In shallow exposures, plagioclase phenocrysts (up to 5 mm in diameter) are euhedral and normally zoned ($An_{40–15}$) partially resorbed tabular crystals, which have strongly sericitized, calcic-bearing cores ($An_{40–25}$). According to Wall *et al.* (1987) this type of alteration in plagioclase is consistent with the early crystallization of an anorthitic core which becomes unstable on cooling and is subsequently hydrothermally altered to sericite and calcite. There are two types of K-feldspar: phenocrysts, up to 20 mm in diameter, containing euhedral to subhedral inclusions of plagioclase ($An_{40–15}$), biotite; and K-feldspar pseudomorphs (up to 10 mm)

	Hydrothermal biotite (greenish -brown color)					Magmatic biotite (dark brown color)				
Sample no.	25-431	25-431	25-431	25-431	34-477	25-514	34-477	34-163	34-164	34-163
Drill core	25	25	25	25	34	25	34	34	34	34
Type	K	K	K	K	Phc	Frs	Phc	phc	K	phc
SiO_2	41.29	39.25	39.03	38.74	41.29	38.58	37.27	37.6	38.58	37.27
TiO_2	2.02	2.17	2.11	3.91	2.02	3.82	4.27	4.95	3.82	4.27
Al_2O_3	15.05	15.5	15.54	15.53	15.05	14.55	13.53	22.86	14.55	13.53
FeO	2.53	4.17	4.18	4.79	2.53	15.69	16.38	13.51	15.69	16.38
MnO	0	0.04	0.01	0.02	0	0.17	0.18	0.06	0.17	0.18
MgO	23.18	21.5	21.58.	21.39	23.18	14.34	14.4	14.39	14.34	14.4
CaO	0	0	0.04	0.04	0	0.03	0.01	0.13	0.03	0.01
Na_2O	0.14	0.18	0.17	0.2	0.14	0.3	0.3	0.09	0.3	0.3
K_2O	10.51	10.43	10.25	10.34	10.51	9.35	9.41	2.26	9.35	9.41
F	2.6	1.96	2.1	1.87	2.6	0.38	0.33	0.38	0.38	0.33
Cl	0.04	0.09	0.08	0.07	0.04	0.2	0.17	0.05	0.2	0.17
Total	97.35	95.29	95.09	96.91	97.35	97.41	96.24	96.29	97.41	96.24
Number of atoms based on 11 0										
Si	2.77	2.75	2.72	2.68	2.77	2.81	2.77	2.72	2.81	2.77
Ti	0.1	0.11	0.11	0.2	0.1	0.21	0.24	0.05	0.21	0.24
AlI	1.2	1.28	1.29	1.27	1.2	1.26	1.2	2.02	1.26	1.2
Fe	0.14	0.24	0.24	0.28	0.14	0.96	1.02	0.84	0.96	1.02
Mn	0	0	0	0	0	0.01	0.01	0	0.01	0.01
Mg	2.32	2.23	2.24	2.2	2.32	1.56	1.6	1.37	1.56	1.6
Ca	0	0	0	0	0	0	0	0.01	0	0
Na	0.02	0,02	0.02	0.03	0.02	0.04	0.04	0.01	0.04	0.04
K	0.9	0.93	0.91	0.91	0.9	0.9	0.89	0.21	0.87	0.89
F	0.55	0.43	0.46	0.41	0.55	0.09	0.08	0.09	0.09	0.08
Cl	0	0.01	0.01	0.01	0	0.02	0.02	0.01	0.02	0.02
F/(F + Cl)	1	0.98	0.98	0.98	1	0.82	0.8	0.9	0.82	0.8
Fe/(Fe+Mg)	0.06	0.1	0.1	0.11	0.06	0.38	0.39	0.38	0.38	0.39
Frs = fresh rock, K = potassic zone, Phc = phyllic zone										
FeO = total Fe										

Table 1. Composition of Magmatic and Hydrothermal Biotite in the Sungun Porphyry Copper Deposit

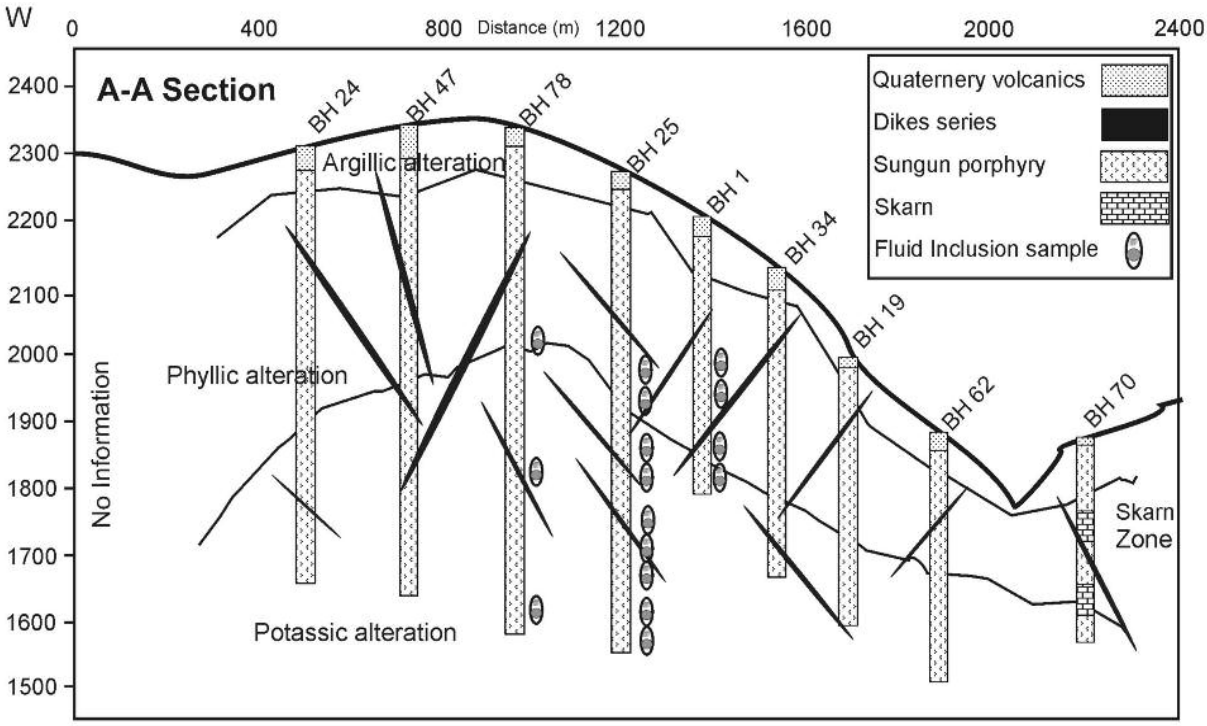

Text-fig. 2. Profile along A-A in Text-fig. 1 illustrating the position of diamond drill holes, dyke series, and the pattern of hypogene alteration zones (potassic, phyllic and argillic) in Porphyry Stock II.

that replaced plagioclase phenocrysts. Biotite phenocrysts are up to 3 mm in diameter and have been altered to chlorite and sericite at shallow depths in the pluton (Hezarkhani 2006a).

Transition alteration (potassic-phyllic)

Potassic alteration is overprinted by a large zone of pervasive transition alteration in the central part of the stock, which grades upwards into phyllic alteration. Transition alteration is characterized by albite replacement of more An-rich plagioclase, and albite rims on orthoclase. Minor sericite and pyrite also partially replaced plagioclase, biotite and hornblende (Text-fig. 6b). A distinguishing characteristic of this type of alteration is the white color of the altered rocks (Hezarkhani and Williams-Jones 1998). This change of colour from the original grey to white reflects a strong depletion of ferromagnesian minerals like hornblende and biotite. The most important change in trace element distribution was the depletion in Cu.

Phyllic alteration

The change from transition to phyllic alteration is gradual and is marked by an increase in the proportion of muscovite. Phyllic alteration is characterized by the replacement of almost all rock-forming silicates by sericite and quartz and overprints the earlier formed potassic and transition zones. Pyrite forms up to 5 vol. percent of the rock and occurs in veins and disseminations. Quartz veins are surrounded by weak sericitic halos (Fig. 6c). Vein-hosted pyrite is partially replaced by chalcopyrite. Silicification was synchronous with phyllic alteration and variably affected much of the stock and most of the dykes. This observation is supported by whole-rock chemical analyses, which show that Si was added in higher amounts than during any other stage of alteration (Hezarkhani and Williams-Jones 1998). In contrast to the transition zone, appreciable Cu was added to the rock during phyllic alteration. It is difficult to separate transition and phyllic alteration because of intense silicification during the latter alteration (Text-fig. 3).

Argillic

Feldspar is locally altered to clay down to a depth of 400 m, and within 80 m of the erosional surface the entire rock has been altered to an assemblage of clay minerals, hematite and quartz. The altered rocks are soft and white coloured. XRD analyses indicate that kaolinite is the dominant phyllosilicate, and that it is accompanied by illite. A shallow level of alteration is in-

terpreted to represent a supergene blanket over the deposit and the deeper clay alteration of feldspar may have had the same origin. However, it is possible that the latter represents an advanced argillic stage of the hypogene alteration.

MINERALIZATION

Hypogene copper mineralization was introduced during potassic alteration and to a lesser extent during phyllic alteration, and exists as disseminations and in veinlet form. During potassic alteration, the copper mineralization was deposited as chalcopyrite and minor bornite; later hypogene copper mineralization deposited mainly chalcopyrite (Text-fig. 3). Hypogene molybdenum mineralization (molybdenite) was concentrated mainly in the deep part of the stock and is associated exclusively with potassic alteration, where it is found in quartz veins accompanied by K-feldspar, anhydrite, sericite and lesser chalcopyrite. Alteration of feldspars and biotite (from potassically altered rocks) was accompanied by an increase in sulphide content outward from the central part of the stock. Copper mineralization increases toward the margins of the central potassic zone, from less than 0.20 wt % to 0.85 wt%. There is also a positive correlation between silicification and copper mineralization. The maximum Cu grade is associated with biotite, orthoclase and sericite (potassic zone), while the pyrite content is highest (3-10 vol % of the rock) in the marginal quartz-sericite (phyllic) zone. The ratio of pyrite to chalcopyrite in the zone of richest hypogene copper mineralization in the potassic alteration zone is as low as 4:1, but toward the margins of the stock the ratio increases to 15:1.

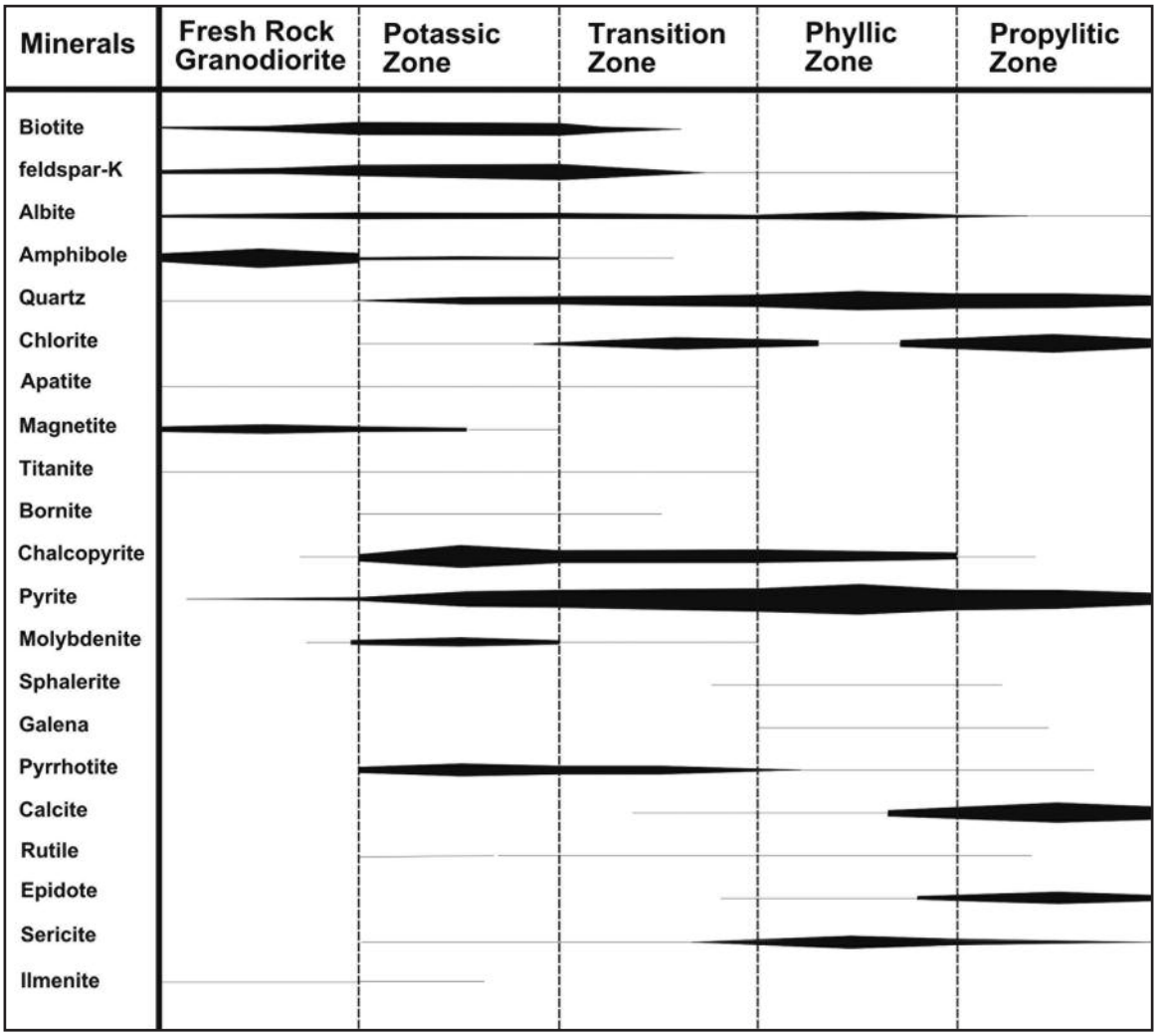

Text-fig. 3. Paragenetic sequence of the development of various alterations in porphyry stock II at Sungun. The thickness of the horizontal bars is related to the relative abundance of the mineral in the porphyry system (Hezarkhani and Williams-Jones 1998; Calagari 2004)

MINERALIZATION STAGES

The Sungun deposit contains well-developed stockwork mineralization that is concentrated in the potassic and transition zones (the transition zone is actually the outermost part of the potassic zone and is characterized by a low content of biotite and abundant sericitization). Based on mineralogy and cross-cutting relationships, it is possible to distinguish four main groups of veins representing four episodes of vein formation: 1) quartz + molybdenite + anhydrite ± K-feldspar with sporadic pyrite, chalcopyrite and bornite, II) quartz + chalcopyrite + pyrite ± molybdenite, III) quartz + pyrite + calcite ± chalcopyrite + anhydrite (gypsum) + molybdenite, IV) quartz, and/or calcite, and/or gypsum ± pyrite (Hezarkhani and Williams-Jones 1998) (Text-fig. 4 and 5).

The stockwork system is dominated volumetrically by group IV and group I veins (up to 21 and 24 % by volume of the rock, respectively). Group II and group III veins occupy up to 15 volume percent and 13 volume percent of the rock, respectively. The integrated vein volumes vary between 0 and 22 percent, and average about 16 percent.

Group I veins are discontinuous, vary in thickness between 0.5 and 3 mm, and formed during the early fracturing of the porphyry stock. Molybdenite is the most important sulphide mineral, and occurs mainly along vein margins; K-feldspar, anhydrite, chalcopyrite, bornite and pyrite occur in the central part of the vein, and less commonly at the margins. Pyrite and chalcopyrite partially replace the molybdenite. Quartz comprises from 60 to 95 percent of the volume of the veins. The veins are surrounded by potassic, and less commonly phyllic and propylitic alteration haloes.

Group II veins generally crosscut and in places offset the group I veins (Text-fig. 6d). The most important characteristics of group II veins are well-developed sericitic alteration haloes and the lack of K-feldspar. The volume ratio of chalcopyrite to pyrite is 2:1. Molybdenite contents vary from traces to less than 5 volume percent of the vein. The alteration haloes are most obvious in the potassic alteration zone, where hydrothermal biotite in the halo was destroyed. The sericitic alteration haloes have thicknesses varying between 1 and 5 mm and have surrounded the quartz veins. Vein quartz is relatively coarse-grained and tends to be oriented perpendicular to the walls of the vein. Sulphide minerals are located mainly in a narrow discontinuous layer in the vein centres, but in some cases sulphides are disseminated through the quartz. Group II veins occur in all alteration zones, but are concentrated mainly in the potassic alteration zone.

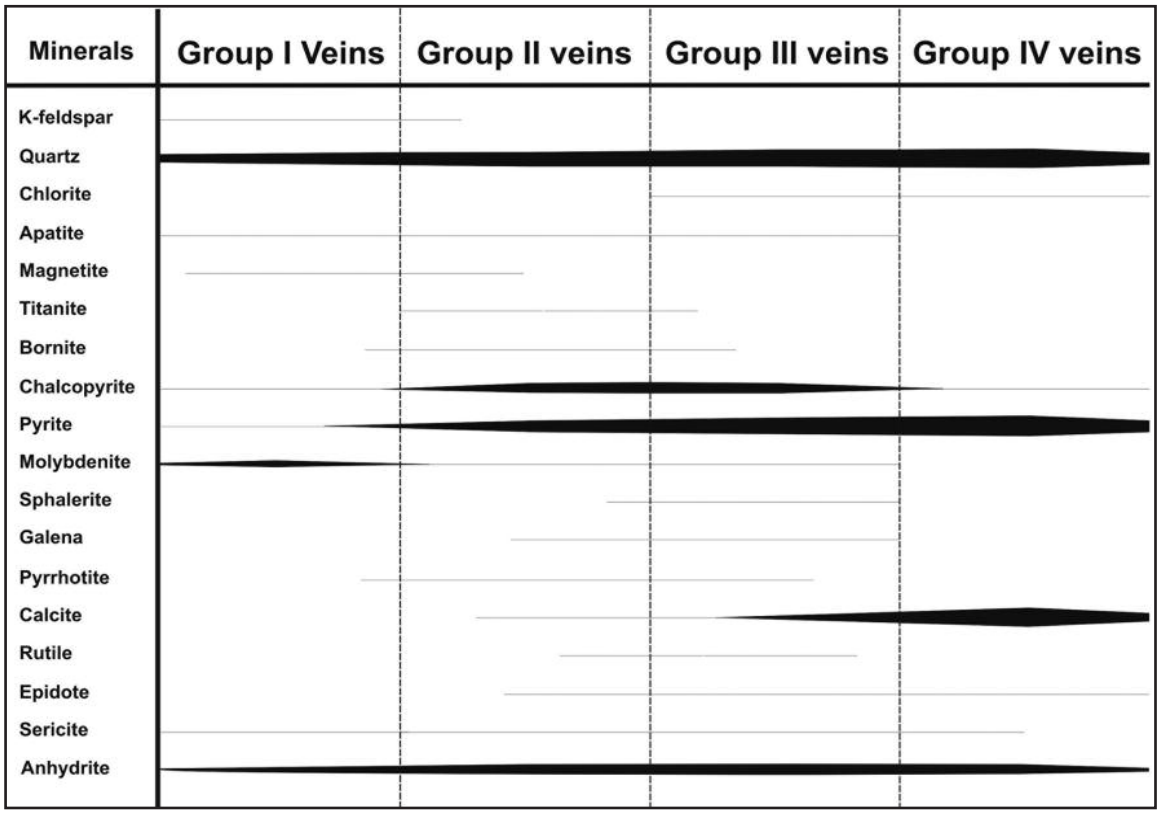

Text-fig. 4: Relative mineral abundances in various veins and veinlets in the Sungun deposit. Widths of bars denote qualitative abundances

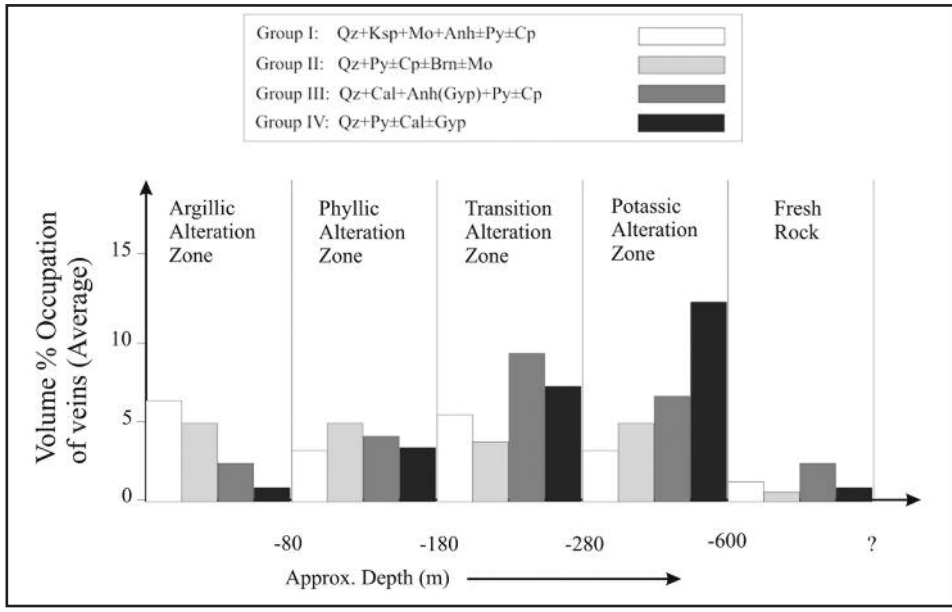

Text-fig. 5. Diagram showing the volume proportions of the different vein groups in each of the alteration zones

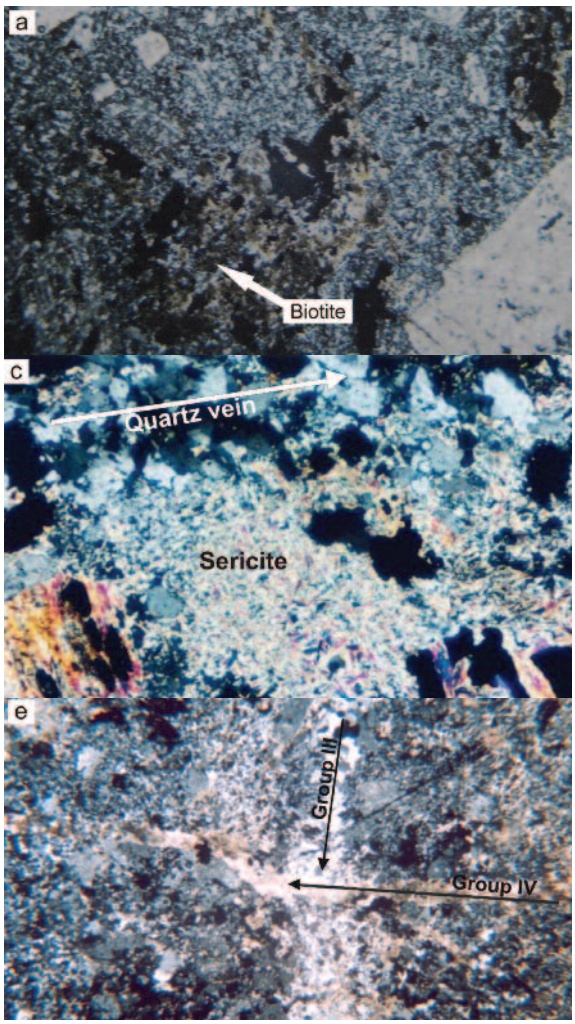

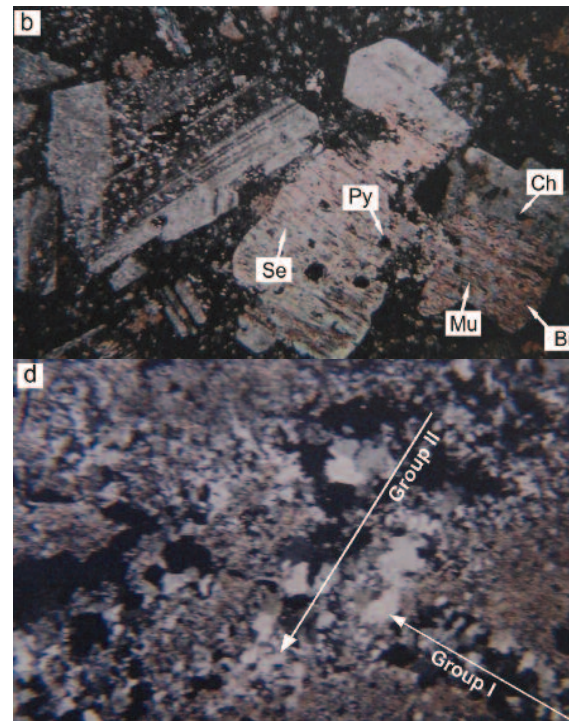

Text-fig. 6. (a) – Ferromagnesian mineral (such as amphibole) are altered to hydrous minerals (such as biotite and muscovite), (b) – There are minor sericite and pyrite which partially replaced plagioclase, and biotite within the sample, (c) – In sample 10 (phyllically altered sample from BH 33; elevation level=1622m) quartz veins are surrounded by weak sericitic haloes, (d) – Group II veins that cutting and offsetting the group I veins, (e) – Group IV veins (calcite vein) are cutting and offsetting the group III veins

Group III veins cross-cut both Group I and II veins, and in some cases offset the earlier-formed veins. Group III veins are most abundant in the phyllic alteration zone, and are relatively continuous, commonly layered and vary in thickness from 3 to 50 mm. Quartz occurs mainly near the vein margins with anhydrite, calcite, and

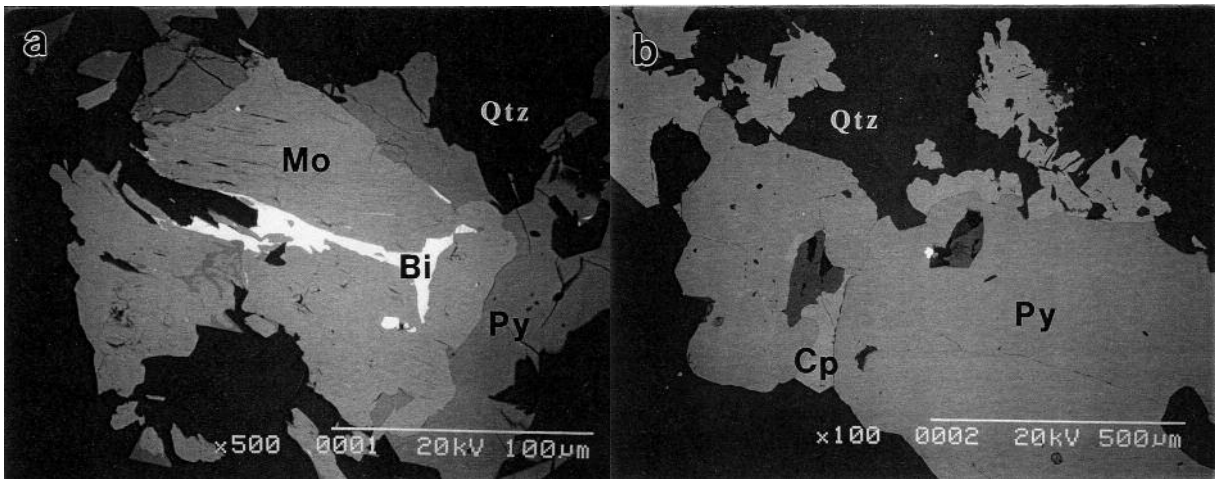

Text-fig. 7. Scanning electron photomicrographs. (a) – Molybdenite with associated anhedral bismuthinite and pyrite. (b) – Quartz associated with pyrite altered to chalcopyrite. All fluid inclusions have been measured from quartz veins associated with ore minerals. Abbreviations: Bi – bismuthinite, Cp – chalcopyrite, Mo – molybdenite, Py – pyrite, Qtz – quartz

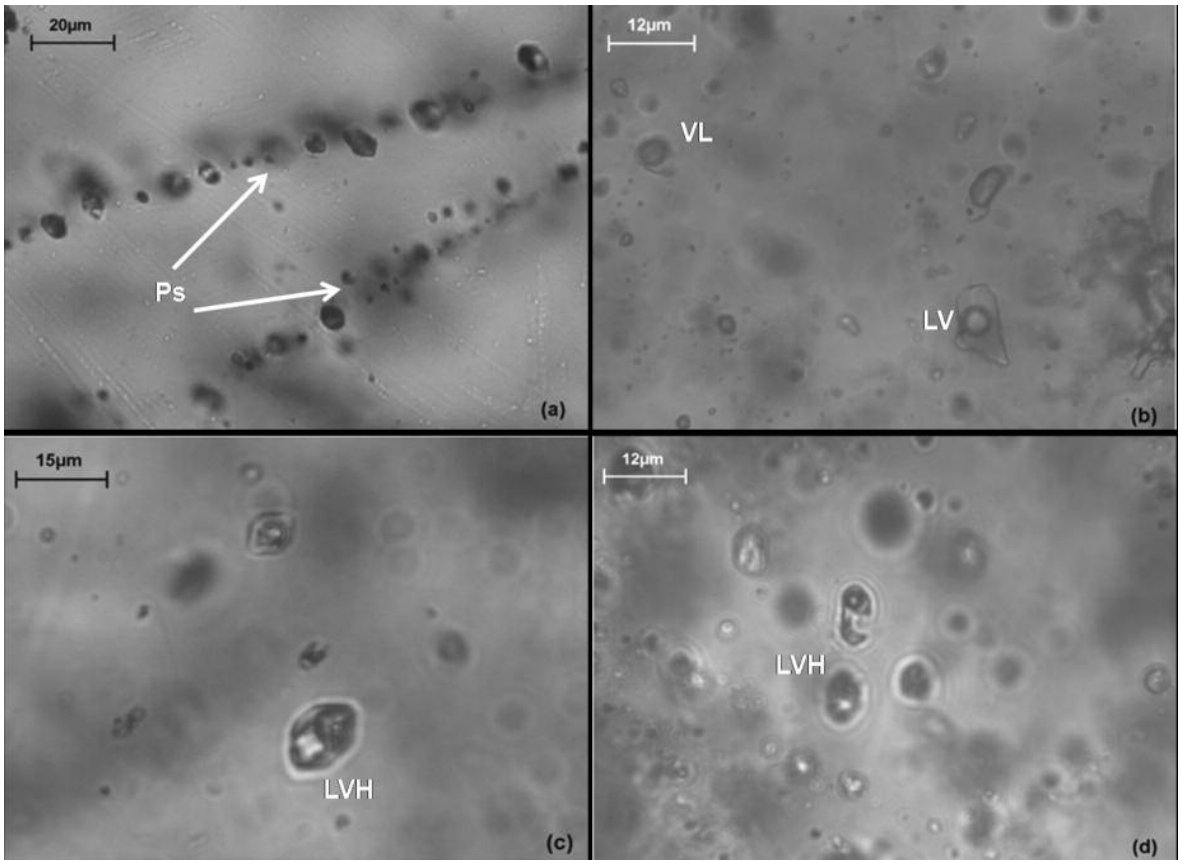

Text-fig. 8. Photomicrographs of different inclusion types within mineralized quartz vein from Sungun. (a) – Secondary fluid inclusions; (b) – Secondary biphase VL inclusions, (c) – primary polyphase inclusion from potassic alteration assemblage (sample no. 42) and (d) – primary inclusion from phyllic alteration assemblage (sample no. 18). All photographs were taken at ambient laboratory temperature. See text for discussion.

Type	Statistical parameter	Salinity (%)	T_H (°C)	T_m (°C)	T_e (°C)	Size (μ^2)	L/V Ratio
P	Mean	31	430	-10.3	-41.3	24.3	3.2
	Standard Deviation	17.3	85	5.1	10.8	9.6	2.5
	Sample Variance	321	7928	28.0	127.4	100.7	6.6
	Minimum	1.1	220	-33	-64.9	6	0.1
	Maximum	65.5	600	-0.5	-14	58	19
S	Mean	20.1	298	-6.3	-32.0	18.9	2.4
	Standard Deviation	15.7	78	4.6	9.9	8.8	2.3
	Sample Variance	293	7229	25.5	116.2	91.8	6.0
	Minimum	1.2	88	-30	-59.3	5.1	0.1
	Maximum	48	437	-0.4	-13.4	58	16.0
Ps	Mean	22.1	303	-8.7	-29.1	17.2	2.2
	Standard Deviation	14.6	72	4.3	9.2	8.1	2.1
	Sample Variance	272	6723	23.7	108.1	85.4	5.6
	Minimum	0.8	215	-27.8	-57.9	5.1	0.1
	Maximum	51.3	588	-0.4	-17	51.3	13.9

Table 2. Statistical parameters of raw data based on fluid inclusion study and microthermometry for 645 measurements on 47 samples, separated based on fluid inclusion types into P: Primary, S: Secondary and Ps: Pseudosecondary

sulphide minerals intergrown in the vein centres. Quartz is relatively coarse-grained, and locally shows optical zoning (overgrowths). The only copper mineral is chalcopyrite, which is observed mainly as small blebs and inclusions in pyrite. Early-formed anhedral to subhedral grains of pyrite are replaced by anhedral grains of chalcopyrite. Group II and III veins appear to have a common origin, with group III veins probably having formed by re-opening of group II veins. As will be discussed in the section on fluid inclusions, primary saline fluid inclusions similar to those in group II veins are present in the centres of zoned quartz crystals in group III veins. The paucity of chalcopyrite and other copper minerals in group III veins suggests that they have been leached by later fluid circulating in these veins.

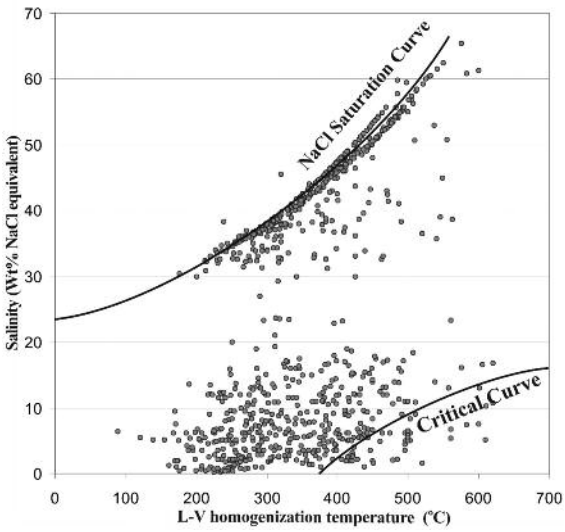

Text-fig. 9. Salinity versus $T_{H(L-V)}$ illustrating the distribution pattern of the data points relative to the NaCl saturation and critical curves (NaCl saturation and critical curves from (Cloke and Kesler 1979). Dashed lines referring to vapour pressures of NaCl solutions at the indicated temperatures and salinity from Roedder (1984)

Group IV veins crosscut all the other vein groups, and represent the youngest vein-forming event in the Sungun stock (Text-fig. 6e). They are very thick (up to 17 cm), and filled by quartz, and/or calcite, and/or gypsum. Group IV veins are found mainly in the propylitic zone, but also occur locally in the phyllic and potassic alteration zones. The only sulphide mineral is pyrite, which occupies about 10 vol. % of these veins. Group IV veins are usually surrounded by zones of silicification up to 3 cm wide.

Quartz crystals exist within almost all types of quartz veinlets (late-type, quartz-sulphide, quartz-molybdenite and early type. Based upon their phase content, three types of inclusion are present at Sungun: (1) vapour-rich 2-phase, (2) liquid-rich 2-phase, and (3) multi-phase solid. Halite crystals are larger than the other solids and can be readily distinguished by their cubic shape. Similar characteristics are seen in fluid inclusion assemblages from other PCDs such as El Salvador, Chile (Gustafson and Hunt 1975), Santa Rita, New Mexico (Ahmad and Rose 1980), Bingham, Utah (Roedder 1971), Yandera and Panguna, Papua New Guinea (Watmuff 1978; Eastoe 1978), Copper Canyon, Nevada (Nash 1976), Bajo de la Alumbrera, Argentina (Ulrich *et al.* 2001).

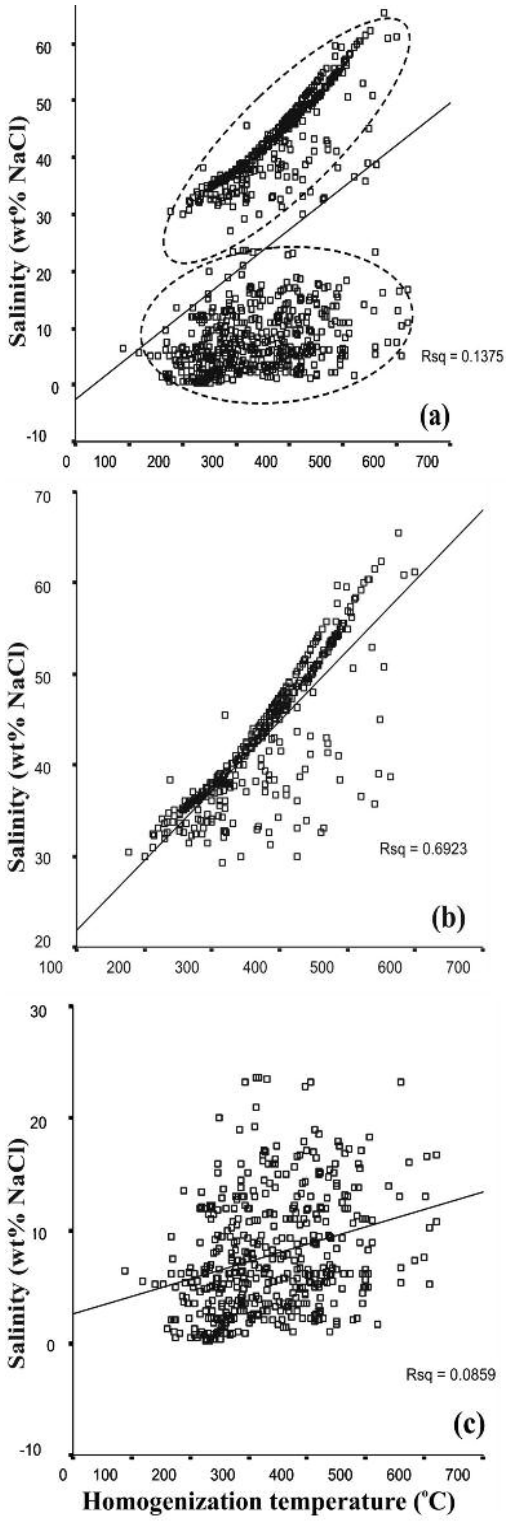

Text-fig. 10. Plot of salinity vs. homogenization temperature showing two different correlations between salinity and Th. (a) – a relatively high correlation between high salinities and Th ($R^2 = 0.6923$, correlation coefficient = 0.83) and a low correlation between low salinities and Th ($R^2 = 0.0859$, correlation coefficient = 0.29)

Fluid inclusions are abundant in quartz of all vein types, and range in diameter from 1 μm up to 15 μm. The majority of inclusions examined during this study had diameters of 4rothermometrically. Only fluid inclusions within the quartz crystals in quartz-sulphide and quartz-molybdenite veinlets were chosen for microthermometric analyses for two important reasons: (1) the inclusions are intimately associated with copper and molybdenum sulphides (Text-fig. 7a, 7b), (2) these veinlets contain inclusions >7μm which allows for more reliable thermometric analysis. The individual quartz crystals contain numerous cross-cutting micro-fractures along which fluid inclusions are aligned (Text-fig. 8a).

Since hydrothermal quartz in the very early veins (group I) was generally too fine-grained to host fluid inclusions of sufficient size for study, most of the observations were restricted to fluid inclusions in coarse-grained quartz of early mineralized veins (group II) and later quartz-anhydrite-pyrite veins (group III). A preliminary classification of fluid inclusions carried out based on the number, nature and relative proportions of phases at room temperature, led to the recognition of the following types of fluid inclusions:

LV inclusions consist of liquid + vapour ± solid phases with the liquid phase volumetrically dominant. These fluid inclusions are common in all mineralized quartz veins, and are abundant in group II and III veins (Text-fig. 8b). The diameters of these fluid inclusions ranges from 3 to 12 μm. LV inclusions are found in all vein groups in variable proportions. They are most abundant in the group II and III veins, and rare in group I veins. Most LV inclusions are distributed along healed fractures, and are of secondary origin.

VL inclusions are found in quartz phenocrysts from fresh rocks and in group I, II and III quartz veins. Some of these inclusions occur in growth zones in

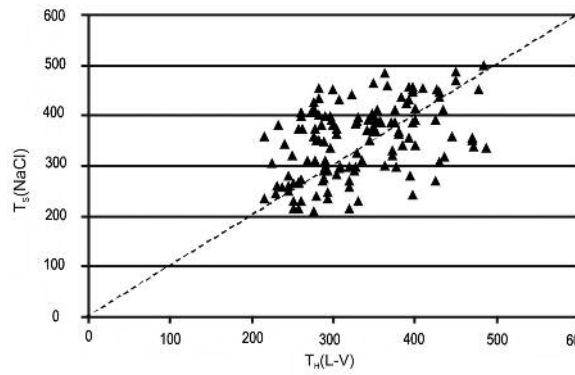

Fig. 11. Liquid-vapour homogenization temperature [$T_{H(L-V)}$] versus halite dissolution temperature [$T_{S(NaCl)}$] for halite-bearing inclusions at Sungun. For calculating the pressure we used points over the diagonal line, where $T_{S(NaCl)} > T_{H(L-V)}$

Statistical parameter	Salinity	Th	T_m	T_e	Size(μm^2)	L/V Ratio
Mean	43	375	-11.6	-46.9	24.5	3.4
Standard Deviation	7.6	82	6.4	9.1	12.4	2.1
Sample Variance	57	6664	40.3	82.5	154	4.3
Minimum	29	176	-33	-67.4	8	0.3
Maximum	65.5	600	-1.2	-26	70	9

Table 3. Descriptive statistics of primary inclusion's data for high salinity inclusions (more than 27 wt% NaCl)

No.	BH No.	Alteration	Elevation(m)	Cu (%)	Th→H(^oC)	Salinity (%)	Th→V(^oC)	Pressure(bar)	Density(gr/cm^3)
1	BH	PHY	1848	0.73	337	39.8	310	398	1.11
2	BH	PHY	1808	0.86	351	42.5	330	367	1.15
3	BH	POT	1801	0.68	394	46.5	377	339	1.12
4	BH	POT	1774	0.64	371	44.8	357	278	1.11
5	BH	POT	1660	0.3	373	45.1	338	555	1.14
6	BH	POT	1615	0.75	362	47.2	328	693	1.19
7	BH	POT	1603	0.63	333	43.1	296	693	1.16
8	BH	POT	1594	0.98	337	41.6	304	490	1.14
9	BH	POT	1581	0.65	347	42.6	330	295	1.12
10	BH	PHY	1622	0.49	460	54.6	454	311	1.13
11	BH	POT	1592	0.7	359	43.3	318	670	1.19
12	BH	POT	1729	0.29	348	45.5	316	629	1.17
13	BH	PHY	1853	0.6	410	46	400	267	1.08
14	BH	PHY	1847	0.52	450	48	435	399	1.07
15	BH	PHY	1843	0.31	430	47.8	417	340	1.08
16	BH	PHY	1830	0.48	312	36	303	154	1.07
17	BH	PHY	1827	0.64	234	33.5	219	212	1.13
18	BH	PHY	1826	0.64	220	33	207	195	1.13
19	BH	PHY	1824	0.85	250	34	233	239	1.12
20	BH	PHY	1876	1.06	350	37	345	124	1.04
21	BH	PHY	1861	0.85	355	38	348	159	1.04
22	BH	PHY	1823	0.57	414	46.9	394	407	1.1
23	BH	PHY	1821	0.71	410	48	403	231	1.1
24	BH	PHY	1818	1.21	423	49	413	287	1.1
25	BH	PHY	1813	1.17	380	36	359	312	1.02
26	BH	PHY	1746	0.85	399	36	395	163	0.97
27	BH	PHY	1741	0.9	428	46	419	281	1.06
28	BH	PHY	1807	0.52	382	38.3	352	435	1.05
29	BH	PHY	1801	0.53	425	46.4	413	316	1.07
30	BH	POT	1707	0.1	356	42	339	285	1.1
31	BH	PHY	1711	0.12	404	46	395	251	1.08
32	BH	POT	1647	0.72	385	45.5	382	144	1.09
33	BH	POT	2080	0.41	461	52.7	436	599	1.13
34	BH	POT	1813	1.31	431	47.7	409	460	1.09
35	BH	POT	1661	0.63	444	49.9	417	576	1.12
36	BH	POT	1780	0.42	442	49.7	421	486	1.11
37	BH	POT	1543	0.23	455	51.1	420	706	1.13
38	BH	PHY	1671	0.76	404	45.4	393	265	1.08
39	BH	POT	1792	0.61	418	47.3	376	716	1.13
40	BH	POT	1685	0.65	583	60.9	561	477	1.13
41	BH	POT	1673	0.32	475	53.6	446	691	1.13
42	BH	POT	1659	0.4	406	46.7	377	523	1.12
43	BH	PHY	1959	0.66	394	45.2	370	417	1.11
44	BH	PHY	1918	0.47	389	44.5	353	578	1.12
45	BH	PHY	1783	0.55	388	43.8	371	308	1.09
46	BH	POT	1676	0.42	462	32.6	426	475	1.14
47	BH	POT	1631	0.79	447	38.5	418	458	0.99

Table 4. Samples from 47 locations in 13 boreholes distinguished into potassic and phyllic. Based on microscopic studies and XRF analysis, 22 of them are defined as potassic and 25 as phyllic alteration

	Descriptive	Elevation	Cu	Th→H	Salinity	Th→V	Pressure	Density
Potassic	Mean	1695	0.57	409	46.3	382	512	1.12
	S.D.	116	0.27	64	5.7	64	163	0.04
	Var.	13351	0.07	4112	32.7	4093	26568	0.002
	Min	1543	0.10	333	32.6	296	144	0.98
	Max	2080	1.31	583	60.9	561	716	1.19
Phyllic	Mean	1811	0.68	376	42.5	361	310	1.08
	S.D.	71	0.25	63	5.8	64	111	0.04
	Var.	5092	0.06	4027	34	4094	12215	0.002
	Min	1622	0.12	220	33	207	130	0.97
	Max	1959	1.21	460	54.6	454	609	1.15
Total	Mean	1757	0.63	391	44.2	371	408	1.1

Table 5. Descriptive statistics of 25 samples from phyllic alteration and 22 samples from potassic alteration

group I and II quartz veins, where they are accompanied by LVH fluid inclusions, indicating that most of them are primary. VL inclusions are generally elongated and have rounded ends, but some have negative crystal shapes. Some of the VL inclusions have variable liquid-vapour ratios, and may have formed from the necking down of LVH inclusions or heterogeneous entrapment of liquid and vapour.

Anhydrite and chalcopyrite did not dissolve on heating to temperatures in excess of 600°C. Chalcopyrite was identified on the basis of its optical characteristics (opacity and triangular cross section) and composition in opened inclusions (SEM-EDAX analyses yielded peaks for Cu, Fe and S). Anhydrite forms transparent anisotropic prisms and was shown by SEM-EDAX analyses to consist only of Ca and S (elements lighter than F could not be analyzed) (Hezarkhani and Williams-Jones 1998).

LVH inclusions are found in all veins, from the deepest, potassically altered part of the stock to the shallow level veins (Text-fig. 8c, 8d). The fluids occupy cavities ranging from 1 μm to 15 μm in diameter. The coexistence of LVH inclusions and vapour-rich inclusions with consistent phase ratios in the growth zones of quartz grains from potassic and phyllic alteration zones suggests their primary origin, and coexistence of two immiscible aqueous fluids.

The majority of LVH inclusions examined during this study had diameters of 4-12 μm. Forty seven sub-surface samples containing quartz veinlets from diamond boreholes holes within the hypogene alteration zones in porphyry Stock II were selected for thermometric analyses.

FLUID INCLUSION STUDIES

The samples were initially prepared for microscopic examination. Based on mineral content, we found the origin of alteration and categorized them into potassic and phyllic. The distribution pattern, shape, size, and phase content of fluid inclusions within the quartz crystals were examined under the microscope (Table 2). The Linkam operating unit was applied to measure the temperatures of phase changes in fluid inclusions; this operates by passing pre-heated or pre-cooled N_2 gas around the sample (Werre *et al*. 1979). Stage calibration was performed using synthetic and/or well-known fluid inclusions. Accuracy at the standard reference temperatures was ±0.2°C at –56.6°C (triple point of CO_2), ±0.1°C at 0°C (melting point of ice), ±2°C at 374.1°C (critical homogenization of H_2O), and ±9°C at 573°C (alpha to beta quartz transition). The heating rate was approximately 1°C/min near the temperatures of phase transitions.

Microthermometric analysis

Thermometric analyses were performed principally on fluid inclusions which were relatively large (>7 μm). Freezing and heating experiment helped determine the approximate salinity (wt% NaCl equivalent) and homogenization temperature (T_H) respectively (Table 2). For undersaturated inclusions, the homogenization temperature of liquid and vapour (either L+V→L or L+V→V) was recorded. In the halite-bearing inclusions, two points: (1) $T_{S(NaCl)}$ (the temperature at which halite dissolves) and (2) $T_{H(L–V)}$ (temperature of vapour and liquid homogenization) were recorded.

Homogenization temperatures

LV fluid inclusions homogenize to liquid T_h (L+V→L) at temperatures between 523° and 298°C. Most VL inclusions homogenize to vapour T_h (V+L→V) between 351° and 600 (°C). The frequency distribution of halite-bearing inclusions homogenizing by halite disappearance ($T_{S(NaCl)} > T_{H(L–V)}$) display a wide range of $T_{S(NaCl)}$ values, varying from 220 to 583 (°C). Salinities based on the halite dissolution

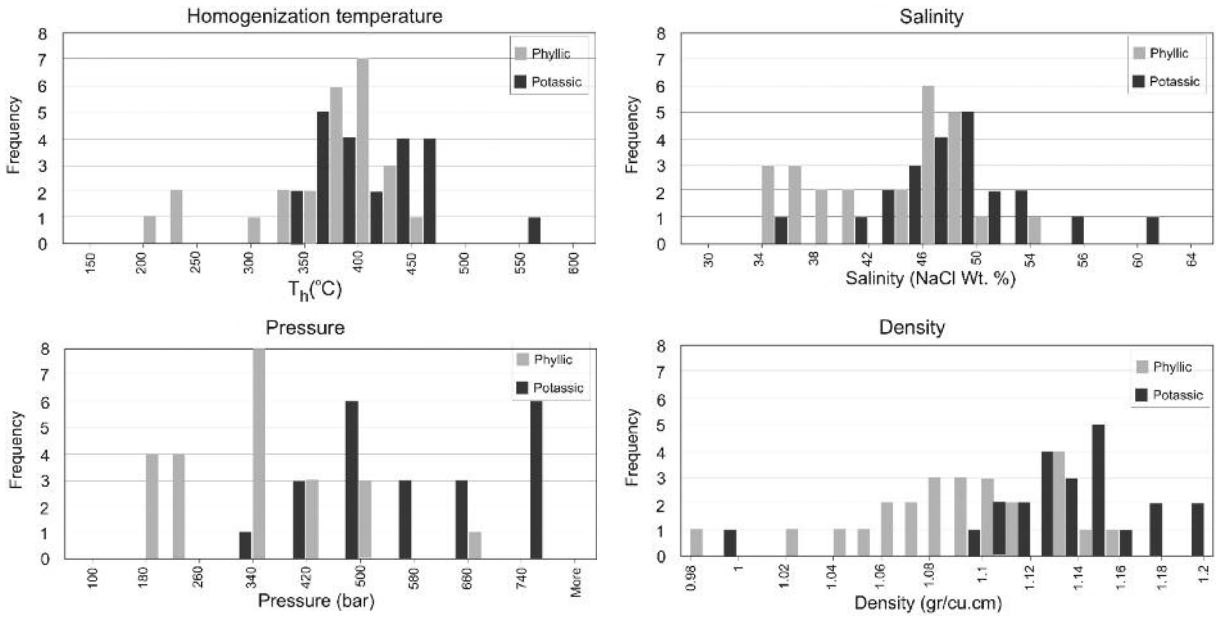

text-ig. 12. Histogram of the homogenization temperature, salinity, pressure and density for 47 analyzed and calculated points based on fluid inclusions. Data shows that there is no sharp boundary between the potassic and phyllic alterations and they seem like two overlapping populations

temperature range from 29.7 to 65.5 wt % NaCl equivalent (Sterner *et al.*, 1988). The halite-bearing inclusions homogenizing by simultaneous disappearance of halite vapour and/or by vapour disappearance ($T_{S(NaCl)} \leq T_{H(L–V)}$) show a similar range of distribution, and their $T_{H(L–V)}$ values vary from 200 to 580 (°C) (Table 4).

Salinity in the inclusion fluids

The temperatures of initial (T_e) and final melting of ice ($T_{m\ ice}$) were measured on LV, VL, and LVH type fluid inclusions. The temperature of initial ice melting (Te) of most LV fluid inclusions was between –23° and –24°C, suggesting that NaCl is the principal salt in solution. The T_e value of VL fluid inclusions ranges from – 20° to –46°C with a mode of ~–22°C, suggesting that Na and K are the dominant cations in the solution, but that there may be another component, for example Mg and Ca. The eutectic temperatures that could be measured in LVH inclusions range from –30° to –64° C, suggesting important concentrations of Fe, Mg, Ca, and/or other components in addition to Na and K in this type of inclusion. The $T_{m\ ice}$ values for LV inclusions range from –5° to –8°C (Table 2), corresponding to salinities of 7 to 11 wt% NaCl equiv. respectively (Sterner *et al.* 1988). The $T_{m\ ice}$ value for VL inclusions varies from –0.4°C to –12°C, which corresponds to a salinity of between 0.8 and 12.2 wt% NaCl equivalent.

Halite-bearing and non-halite-bearing liquid-rich inclusions at Sungun exhibit a wide variation in salinity, ranging from 0.2 to 65.5 wt% (Text-fig. 9).

As shown by Text-fig. 10a, the fluid inclusions can be sharply divided into 2 populations: low salinity (less than 27 wt% NaCl) and high salinity (between 27 wt% and 65.5 wt% NaCl). In high salinity fluid inclusions (Text-fig. 10b), there is good correlation between the salinity and their homogenization temperature correlation coefficient is around 84 percent (R^2=0.69). In low salinity fluid inclusions (Text-fig. 10c), the salinity and the homogenization temperature do not show any significant relationship (R^2=0.09). There are many halite-bearing fluid inclusions which have $T_{S(NaCl)} > T_{H(L–V)}$, and the discrepancy between $T_{S(NaCl)}$ and $T_{H(L–V)}$ in some inclusions may reach ~42°C (Text-fig. 11). These inclusions may suggest entrapment of supersaturated (with respect to NaCl) fluid or high pressure conditions of entrapment (Table 4, No. 39). However, there are still many halite-bearing inclusions whose data points lie around and below the halite saturation curve ($T_{S(NaCl)} < T_{H(L–V)}$) (Text-fig. 11) which, in turn, denotes trapping of saturated and under saturated fluids respectively.

Since we presume that these types of inclusions (LVH) in most quartz veins are primary, and we use data on inclusions with salinities more than 27 wt% NaCl equiv. in our model (to calculate the pressure and the density), based on the Brown and Lamb (1989) method of measuring the geological pressure, the fluid inclusions are considered to be halite- and gas-bearing with high salinity. Table 3 shows the statistical properties of the primary fluid inclusions with salinities more than 27 wt% equivalent.

The pressure and hydrothermal fluid density in the $NaCl-H_2O$ system is calculated for 47 samples using 3 parameters including Th→Halite (°C), Th→Vapour (°C) and salinity (wt% NaCl), based on the BROWN & LAMB (1989) equation using Flincor software (BROWN et al, 1989). Fluid pressures varies from 120 to 720 bars (Table 4)

Boiling

The ascending fluids forming the quartz-sulphide and quartz-molybdenite veinlets began to boil at a temperature of 560°C, based upon fluid inclusion data. The evidence for this process would be: the intimate coexistence of the gas-dominated 2-phase, the moderate salinity liquid-rich 2-phase, and high salinity halite-bearing multi-phase inclusions, homogenizing over the same temperatures (Calagari 2004). In order to reach a high salinity (more than 27 wt % NaCl), to account for the salinity of the co-existing halite-bearing inclusions, substantial heat supply was required during the boiling event; the cooling pluton could provide such a source. As the boiling process continued, the liquid phase became increasingly more saline. Hence, successive generations of inclusions trapped fluids with a higher salinity. Boiling events recurred episodically until the fluid temperature decreased to about 220°C (Text-fig. 9), resulting in the multi-phase hydrofracturing events.

COMPARING THE RESULTS IN TWO ALTERATIONS

As discussed earlier, the analyses were done on the three-phase fluid inclusions that were in the quartz veins adjacent to the mineralization (in different alterations). As we expected, these fluid inclusions show high salinity. With the results presented in Table 5 it could be seen that the average salinity in potassic alteration is slightly higher than the average salinity of the phyllic alteration. However, they are very close to each other, as mentioned in Hezarkhani and Williams-Jones (1998).

The results show that the average of Th, salinity, pressure and density of fluids in the quartz veinlets of potassic alteration are higher than those in phyllically altered samples. Histograms of variables from forty-seven samples shows that no variable could clearly separate potassic and phyllic alterations (Text-fig. 12).

In potassic alteration, the average of homogenization temperature is 414°C, while in phyllic alteration it is 376°C, i.e., there is not much difference between them.

1. The salinity of the hydrothermal fluid has a high correlation with homogenization temperatures, so the average amount of salinity in potassic samples is 46.3 (wt% NaCl), which is slightly higher than that of the phyllic samples (42.5 wt% NaCl). As discussed above, the analyses were done on the three-phase fluid inclusions and, as expected, this type of fluid inclusion shows high salinity in both alterations.
2. Based on the position of the potassic alteration located beneath the phyllic alteration, we expect that the lithostatic pressure was higher in it than in the phyllic one: the average of pressure in the potassic alteration is 512 (bar), while the pressure average in the phyllic alteration is about 310 (bar).The maximum pressure of fluid entrapment can be calculated from the estimated thickness of the overlying rock column at the time of intrusion, which at Sungun is estimated to have been between 1.5 to 2.0 km. The latter represents about 500 m of Cretaceous limestone, plus 1,000 to 1,500 m of lower Tertiary volcanics, volcanoclastic, and related sedimentary rocks. This corresponds to estimated pressure values obtained from fluid inclusion studies.
3. Since these fluid inclusions have the salinities below 27 wt% NaCl equiv. we did not consider them in our results, so their densities were not of interest to us. The density depends on the amount of the salinity of hydrothermal fluid, so the average density of the samples in the potassic alteration is 1.124 (gr/cm^3) which is higher than in the phyllic alteration(1.083 gr/cm^3).

SUMMARY AND CONCLUSIONS

The Sungun deposit is a porphyry system in which the potassic and phyllic alterations contain abundant copper sulphide minerals. The primary multiphase inclusions within the quartz crystals in quartz-sulphide and quartz-molybdenite veinlets (quartz associated with sulphide minerals) were chosen for microthermometric studies and considered to be suitable for calculation of the pressure during the time of origin and the hydrothermal fluid density. Early hydrothermal alteration produced a potassic assemblage (orthoclase-biotite) in the central part of the Sungun stock, propylitic alteration occurred contemporaneously with potassic alteration. In the peripheral parts of the stock, and in a later stage phyllic alteration occurred, overprinting these earlier alterations. Based on fluid inclusion studies in the Sungun deposit, potassic alteration and associated Cu mineralization were produced by a high temperature and high salinity fluid of dominantly magmatic origin. The early hydrothermal fluids are represented by

high temperature (337°C to 583°C), high salinity (up to 60 wt% NaCl equiv.) liquid-rich fluid inclusions, and high temperature (320°C to 550°C), low-salinity, vapour-rich inclusions. Phyllic alteration and copper leaching resulted from the inflow of oxidized and acidic meteoric waters with decreasing temperature (ranging from 220-460°C, with a mean of 376°C) of the system.

The average of all four measured variables (homogenization temperature, salinity, pressure and density) is higher in samples from potassic zones than in those from phyllic ones, but it is not possible to separate the two alterations in graphs. This means that the thermodynamic conditions for the origin of these alterations were close to each other and that other parameters such as fO_2 and pH could affect the mineral precipitation and mineral assemblages in the alterations.

Acknowledgments

The Nicico Copper Company provided access to the deposit and logistic support, including transport and accommodation. Financial support for the research was provided by Amirkabir University of Technology. We would like to thank Dr Farshad Rashidinejad and Mr. Vahid Rafiee for their helpful supports.

REFERENCES

Ahmad, S.N. and Rose, A.W. 1980. Fluid inclusions in porphyry and skarn ore at Santa Rita, New Mexico. *Economic Geology*, **75**, 229–250.

Beane, R.E. and Bodnar, R.J. 1995. Hydrothermal fluids and hydrothermal alteration in porphyry copper deposits. In: Wahl, P.W. and Bolm, J.G. (Eds), Porphyry Copper Deposits of the American Cordillera, Tucson, Arizona, Arizona Geological Society, Arizona, pp. 83–93.

Beane, R.E. and Titley, S.R. 1981. Porphyry copper deposits, alteration and mineralization, part II. *Economic Geology*, **75**, 235–269.

Berberian, M. 1983, the southern Caspian: A compressional depression floored by a trapped, rnodified oceanic crust. *Canadian Journal of Earth Sciences*, **20**, 163-183.

Berberian, M. and King, G.C. 1981. Towards a paleogeography and tectonic evolution of Iran. *Canadian Journal of Earth Sciences*, **18**, 210–265.

Bloorn, M.S. 1981. Chemistry of inclusion fluids: Stockwork Molybdenum deposits from Questa, New Mexico, and Hudson Bay Mountain and Endako, British Columbia. *Economic Geology*, **76**, 1906–1920.

Brown, P.E. 1989. FLINCOR: a microcomputer program for the reduction and investigation of fluid inclusion data. *American Mineralogist*, **74**, 1390–1393.

Brown, P.E. and Lamb, W.M. 1989. P- V-T properties of fluids in the system H,O-CO,-NaCI: New graphical presentations and implications for fluid inclusion studies. *Geochimica et Cosmochimica Acta*, **53**, 1209–1221.

Burnham, C.W. 1979. Magmas and hydrothermal fluids: in Geochemistry of Hydrothermal ore deposits, pp. 71–136. H. L. Barnes, Jon Wiley & Sons, Inc.

Calagari, A.A. 1997. Geochemical, stable isotope, noble gas, and fluid inclusion studies of mineralization and alteration at Sungun porphyry copper deposit, East Azarbaidjan, Iran: Implication for genesis. Unpublished PhD Thesis. Manchester University, Manchester, p. 537

Calagari, A.A. 2004. Fluid inclusion studies in quartz veinlets in the porphyry copper deposit at Sungun, East-Azarbaidjan, Iran. *Journal of Asian Earth Sciences*, **23**, 179–189

Chivas, A.R. and Wilkins, W.T. 1977. Fluid inclusion studies in relation to hydrothermal alteration and mineralization at the Koloula porphyry copper prospect, Guadalcanal. *Economic Geology*, **72**, 153–169.

Cloke, P.L. and Kesler, S.E. 1979. The halite trend in hydrothermal solutions. *Economic Geology*, **74**, 1823–1831.

Dilles J.H. and Einaudi M.T. 1992. Wall-rock alteration and hydrothermal flow paths about the Ann-Mason porphyry copper deposits, Nevada—a 6-km vertical reconstruction. *Economic Geology*, **87**, 1963–2001.

Emami, M.H. and Babakhani, A.R. 1991. Studies of geology, petrology, and litho-geochemistry of Sungun Cu–Mo deposit, Iranian Ministry of Mines and Metals, p. 61.

Etminan, H. 1977. The discovery of porphyry copper–molybdenum mineralization adjacent to Sungun village in the northwest of Ahar and a proposed program for its detailed exploration. Confidential Report, Geological Report, Geological Survey of Iran, p. 26

Gustafson, L.B. and Hunt, J.P. 1975. The porphyry copper deposit at El Salvador, Chile. Economic Geology, **70**, 875–912.

Hedenquist J.W. and Richards J.P. 1998, The influence of geochemical techniques on the development of genetic models for porphyry copper deposits. In: Richards JP, Larson P.B. (Eds), Techniques in hydrothermal ore deposits geology. *Review of Economic Geology*, **10**, 235–256

Heinrich, C.A. 2005. the physical and chemical evolution of low-salinity magmatic fluids at the porphyry to epithermal transition: a thermodynamic study. *Mineralium Deposita*, **39**, 864–889.

Heinrich C.A., Pettke T., Halter W.E., Aigner-Torres M., Audetat A., Gunther D., Hattendorf B., Bleiner D., Guillong M. and Horn I. 2003, Quantitative multi-element analysis of minerals, fluid and melt inclusions by laser-ablation inductively-coupled-plasma mass-spectrometry. *Geochimica et Cosmochimica Acta*, **67**, 3473–3497.

Hezarkhani, A. 2006a, Petrology of Intrusive rocks within the Sungun Porphyry Copper Deposit, Azarbaijan, Iran. *Journal of Asian Earth Sciences*, **73**, 326–340.

Hezarkhani, A. 2006b. Alteration/Mineralization and Controls of Chalcopyrite Dissolution/Deposition in the Raigan Porphyry System, Bam-Kerman, Iran. *Journal of International Geology Review, California*, **48**, 561–572.

Hezarkhani, A., Williams-Jones, A.E. and Gammons, C.H. 1999. Factors controlling copper solubility and chalcopyrite deposition in the Sungun porphyry copper deposit, Iran. *Mineralium Deposita*, **34**, 770–783.

Hezarkhani, A. and Williams-Jones, A.E. 1998. Controls of alteration and mineralization in the Sungun porphyry copper deposit, Iran: Evidence from fluid inclusions and stable isotopes. *Economic Geology*, **93**, 651–670.

Kehayov R., Bogdanov K., Fanger L., von Quadt A., Pettke T. and Heinrich C.A. 2003. The fluid chemical evolution of the Elatiste porphyry Cu–Au–PGE deposit, Bulgaria. In: Eliopoulos D.G. (Ed.), Mineral exploration and sustainable development, pp. 1173–1176. Millpress; Rotterdam.

Mehrpartou, M. 1993. Contributions to the geology, geochemistry, ore genesis and fluid inclusion investigations on Sungun Cu-Mo porphyry deposit, northwest of Iran. Unpublished PhD Thesis. University of Hamburg, Germany, p. 245

Nash, J.T. 1976. Fluid inclusion petrology, data from porphyry copper deposits and applications to exploration. *United States Geological Survey, Professional Paper*, **907-D**, p. 16.

Quan, R.A., Cloke, P.L. and Kesler, S.E. 1987. Chemical analyses of halite trend inclusions from the Granisle porphyry copper deposit, British Columbia. *Economic Geology*, **82**, 1912–1930.

Redmond P.B., Einaudi M.T., Inan E.E., Landtwing M.R. and Heinrich C.A. 2004. Copper deposition by fluid cooling in intrusion centered systems: new insights from the Bingham porphyry ore deposit, Utah. *Geology*, **32**, 217–220.

Roedder, E. 1971. Fluid inclusion studies on the porphyry copper-type ore deposits at Bingham (Utah), Butte (Montana), and Climax (Colorado). *Economic Geology*, **66**, 98–120.

Roedder, E. 1984. Fluid inclusions. *Reviews in Mineralogy*, **12**, p. 644.

Roedder, E. and Bodnar, R.J. 1980. Geologic pressure determination from fluid inclusion studies. *Annual Review of Earth and Planetary Science*, **8**, 263–301.

Shahabpour, J. and Doorandish, M. 2007. Mine drainage water from the Sar Cheshmeh porphyry copper mine, Kerman, IR Iran. Environ Monit Assess, Accepted: 4 July 2007

Shahabpour, J. 1982. Aspects of alteration and mineralization at the Sar-Cheshmeh copper-molybdenum deposit, Kerman, Iran. Ph.D. thesis, Leeds University, 342 p.

Sillitoe R.H. and Hedenquist J.W. 2003. Linkages between volcanotectonic settings, ore-fluid compositions and epithermal precious metal deposits. In: Simmons S.F., Graham I. (Eds), Volcanic, geothermal and ore-forming fluids: rulers and witnesses of processes within the earth. Economic Geology, Special Publication, p. 343.

Sillitoe R.H. 1997. Characteristics and controls of the largest porphyry copper–gold and epithermal gold deposits in the circum- Pacific region. *Austral Journal of Earth Sciences*, **44**, 373–388.

Sourirajan, S. and Kennedy, G.C. 1962. The system H_2O–NaCl at elevated temperatures and pressures. *American Journal of Science*, **260**, 115–141.

Sterner, S.M., Hall, D.L. and Bodnar, R.J. 1988.Synthetic fluid inclusions. V. Solubility of the system NaCI-KCI-H_2O under vapor-saturated conditions. *Geochimica et Cosmochimica Acta*, **52**, 989–1005.

Stocklin, J.O. 1977.Structural correlation of the Alpine ranges between Iran and Central Asia. *Memoir Hors Service Societe Geologique France,* **8**, 333-353.

Tosdal R.M. and Richards, J.P. 2001.Magmatic and structural controls on the development of porphyry Cu±Mo±Au deposits. In: Richards, J.P. and Tosdal, R.M. (Eds), Structural controls on ore genesis. Reviews in Economic Geology, pp 157–180

Ulrich, T., Gunther, D. and Heinrich, C.A. 2001. The evolution of a porphyry Cu–Au deposit, based on La-ICP-MS analysis of fluid inclusions, Bajo de la Alumbrera, Argentina. *Economic Geology*, **96**, 1743–1774.

Urusova, M.A. 1975. Volume properties of aqueous solutions of sodium chloride at elevated temperatures and pressures. *Russian Journal of Inorganic Chemistry*, **20**, 1717–1721.

Wall, V.L., Clemens, J.D. and Clarke, D.B. 1987. Models for granotoid evolution and source composition. *Journal of Geology*, **6**, 731–749.

Watmuff, G. 1978. Geology and alteration-mineralization zoning in the central portion of the Yandera porphyry copper prospect, Papua New Guinea. *Economic Geology*, **73**, 829–856.

Manuscript submitted: 5th January 2008
Revision version accepted: 10th November 2008